

1 **Supporting information.**

2

3 **Section 1: Genotyping by Sequencing**

4 Whole genomic DNA was extracted using the EZNA tissue DNA extraction kit
5 (Omega Bio-Tek) and quantified on a fluorimeter with PicoGreen (Life Technologies Inc.).
6 Reduced complexity single-end libraries were created from the extracted DNA using PstI
7 restriction enzyme digestion at the Cornell Institute for Genomic Diversity (IGD) following
8 the protocol described in (1). One hundred and forty-four *Lepidothrix* individuals and 46
9 individuals from other avian species unrelated to this project were divided into two libraries
10 with 95 individuals uniquely barcoded per library. Each library was single-end sequenced to
11 100 bp on a single lane of an Illumina HiSeq 2000 platform with 95 barcoded samples
12 multiplexed per lane. Each library produced around 200Gbp of unfiltered data.

13 Raw sequence reads were processed using the Stacks 1.44 pipeline (2) to obtain single
14 nucleotide polymorphism (SNP) datasets. The process_radtags module was used to trim raw
15 reads to 90 bp (-t 90) and remove low quality reads (-q option) and reads with uncalled sites
16 (-c). Only reads with high quality scores (Phred33 quality score) and with the correct barcode
17 were retained. Any part of the common adaptors that remained within the 90 bp fragments
18 were removed using fastx_clipper from the FASTX-Toolkit v 0.0.14
19 (http://hannonlab.cshl.edu/fastx_toolkit). Fragments were aligned to the *Lepidothrix*
20 *coronata* reference genome (Warren and McDonnell Genome Institute, 2016) using
21 Bowtie2-2.2.6 (3) with the default values for the “sensitive” setting. We then used the
22 ref_map wrapper script of Stacks to call genotypes. All settings were kept at their default
23 values except the bounded - error SNP calling model was used which estimates the
24 sequencing error rate at each nucleotide position, but does not allow the rate to exceed 0.05.
25 Using vcftools 0.1.15 (4) we filtered for a minimum depth of coverage of at least 10x,
26 retained only biallelic SNPs, and excluded SNPs with average depth of coverage exceeding
27 the 95th percentile and with heterozygosity exceeding 0.75.

28 Three datasets were generated that differ in subsequent filtering strategy. Dataset 1
29 further excluded loci with a locus coverage of less than 50% and individuals with more than

30 70% missing data. This dataset was used for haplotype analyses to estimate coancestry and
31 included 16,281 loci with one or more SNPs for 36 individuals. Dataset 2 was the same as
32 dataset 1, but SNPs were thinned to a minimum distance of 50 kbp. This filtering resulted in
33 a dataset with 7,394 SNPs and 120 individuals and was used for most genetic analyses except
34 as indicated.

35 Dataset 3 filtered SNPs for use in coalescent modelling. Given the proximity of
36 their geographic distributions, we consider the populations of *L. nattereri* distributed East
37 of the Tapajós and Juruena rivers to be the most likely population to have played a role in
38 the formation of *L. vilasboasi*. We therefore excluded individuals of *L. nattereri* found west
39 of the Tapajós/Juruena rivers from these analyses. We also excluded all individuals from
40 the Xingu/Teles Pires headwaters contact zone in which genetically admixed individuals of
41 *L. nattereri* and *L. iris eucephala* occurred. The 84 included individuals were pooled by
42 species and loci not present in at least 25% of individuals in each species were excluded.
43 We next calculated pairwise linkage disequilibrium (r^2) in vcftools separately for each of
44 the three species for SNPs with data present for 12 to 15 individuals per species. We used
45 the R function LDit (code located:
46 https://github.com/rossibarra/r_buffet/blob/master/LDit.r) to fit the observed decay in
47 linkage disequilibrium as a function of physical distance along reference genome contigs
48 (Fig. S1). These decay curves show that r^2 rapidly reached its expected values (with the
49 expectation equal to the inverse of the number of individuals; expectation = 1/12 to 1/15) in
50 less than 5 kbp for all three species, indicating that SNPs as close as 5000bp can be
51 considered statistically independent. Nevertheless, we used a more conservative threshold
52 of 10 kbp and used vcftools to thin SNPs so they were >10 kbp from each other and > 10
53 kbp from coding regions. This thinning both greatly reduces the chances for linkage
54 disequilibrium among our retained SNPs and reduces the chance that retained SNPs will be
55 influenced by loci under selection. We then used a custom R script to down sample each of
56 the three species so that a total of 12 *L. iris*, 10 *L. vilasboasi* and 20 *L. nattereri* gene copies
57 with the greatest depth of coverage (and thus the most robust genotype calls) were retained
58 for each SNP. The resulting dataset had 10,298 SNPs and no missing data.

59

60

61

62 **Section 2: Genetic analyses of population structure and admixture**

63 Assessment of genetic structure across the complex, and the admixed origin of *L.*
64 *vilasboasi*, was performed using several methods on genome-wide SNP data. First, principal
65 coordinate analysis (PCoA), was used to determine the number of genetically distinct clusters
66 and whether *L. vilasboasi* was genetically intermediate between *L. iris* and *L. nattereri* (Fig.
67 2A). Genotypes were coded as 0 and 2 for homozygotes and 1 for heterozygotes and the
68 PCoA was performed on Euclidean distances with the software package PAST 3.01 (5)
69 Second, we performed Bayesian analysis of population structure and admixture using the
70 program Structure 2.3.4 (6). Analyses were conducted using the admixture model and default
71 settings with correlated allele frequencies. Analyses were performed with the number of
72 populations (K) ranging from 1 through 6, and with 30 replicates per K (each with a different
73 random seed and starting parameters). The burn-in period was set to 100,000 and 1,000,000
74 post-burn-in iterations were used, with a sample retained every 100 iterations. For our method
75 of choosing the optimal K see Section 3 below. Third, a phylogenetic network was calculated
76 in SplitsTree 4.14.4 (9) in order to visualize reticulation in the evolutionary history of the
77 three species (Fig. 2C). The NeighborNet method was used to construct the network from
78 uncorrected P distances and equal angle splits. Fourth, we calculated F_{st} and co-ancestry.
79 Dataset 2 was used to calculate genome-wide pairwise Hudson's F_{st} (10) using custom
80 scripts for 4208 SNPs from Dataset 2 for which a further minor allele frequency filter of
81 0.025 was applied. The single sequenced individual of *L. iris iris* and individuals of both *L.*
82 *iris* and *L. nattereri* from the contact zone (Fig. 1) were excluded. The 95% confidence
83 intervals were calculated using 1000 bootstraps (Table S1). Co-ancestry values were
84 calculated in fineRADstructure (11) for the 12 individuals per species with the highest
85 coverage and least amount of missing data from Dataset 1. Co-ancestry quantifies the shared
86 genetic history among individuals across the genome. If *L. vilasboasi* is of hybrid origin
87 between *L. nattereri* and *L. iris*, then we expect that it will have higher co-ancestry and lower
88 F_{st} with both of these species than *L. nattereri* and *L. iris* will with each other. We used a
89 one-tailed t-test to test this prediction for coancestry, and 1000 bootstrapped datasets for F_{st} .

90

91 **Table S1** Mean and 95% confidence intervals for Hudson's F_{ST} (below diagonals) and co-ancestry
 92 (above diagonals) for genome-wide SNP data.

93

	<i>vilasboasi</i>	<i>iris eucephala</i>	<i>nattereri</i> (East)
<i>vilasboasi</i>	-	384.5 (383.5-385.5)	377.4 (376.6-378.2)
<i>iris eucephala</i>	0.178 (0.167-0.189)	-	366.7 (366.0-367.4)
<i>nattereri</i> (East)	0.143 (0.136-0.152)	0.208 (0.198-0.218)	-

94

95

96 Fifth, we compared observed heterozygosity and hybrid indexes of *L. vilasboasi* and
 97 other hybrid populations to that of the parental species. Haffer (12) proposed that *L.*
 98 *vilasboasi* represents a rare hybrid phenotype between *L. iris* and *L. nattereri*. If true, then
 99 we expect to find a large proportion of *L. vilasboasi* individuals representing early
 100 generation hybrids (F_1 , F_2 and backcrosses of F_1 individuals with the parental species) with
 101 both high heterozygosity and genome-wide hybrid indices close to 0.5 for F_1 and F_2 hybrid
 102 classes, or 0.25 for $F_1 \times L. nattereri$ and 0.75 for $F_1 \times L. iris$. In contrast, if *L. vilasboasi*
 103 represented a hybrid species that has persisted over many generations, then interspecific
 104 heterozygosity should have stabilized to a low value across individuals as alternative alleles
 105 inherited from *L. nattereri* and *L. iris* sorted in the resulting population. We used the
 106 admixture values obtained from the analysis of population structure using $K = 2$ for our
 107 hybrid index (0 = pure *L. nattereri*; 1 = pure *L. iris*) and calculated heterozygosity of all
 108 individuals in the R package INTROGRESS 1.2.3 (13) for 353 SNPs from Dataset 1 that
 109 had less than 50% missing data for each parental population (non-contact zone populations
 110 of *L. nattereri* east of the Tapajós/Juruara rivers and *L. iris eucephala*) and for which
 111 parental populations had allele frequency differences exceeding 0.25. The expected hybrid
 112 index for an F_1 and F_2 hybrids would be close to 0.5 while a back cross of a F_1 to a pure *L.*
 113 *nattereri* would be close to 0.25 and to a pure *L. i. eucephala* would be close to 0.75. To
 114 determine the heterozygosity expected for these early generation hybrid classes we used a
 115 custom R script to simulate 5000 F_1 , F_2 and F_1 -*nattereri* and F_1 -*iris* backcrosses using our

116 sample of parental *L. nattereri* and *L. iris* and calculated the observed heterozygosity for
 117 each (see Fig. S3).

118 To assess population structure and admixture with the mtDNA dataset a haplotype
 119 network was constructed using statistical parsimony (14) in the R package pegas (15).

120

121 Section 3: Choosing the optimal number of populations

122 The Evanno method (7) as implemented in the program Structure Harvester (8) has
 123 become the standard approach for choosing the optimal number of populations, K , for
 124 Bayesian analysis of population structure. The Evanno method first calculates $L(K)$ for K 1
 125 to n . $L(K)$ is the mean of the log likelihood of the data at each MCMC step minus half of
 126 the variance across steps. Then $\Delta K = \text{mean}[-2L(K) + L(K-1) + L(K+1)] / \text{stdev}[L(K)]$.

127 The best K is the one with the largest ΔK . While this approach worked well for the simple
 128 examples tested by Evanno et al (7) where $L(K)$ generally increased or leveled off with
 129 increasing K , the approach may fail to detect the correct K following a sudden drop in $L(K)$
 130 as K increases. The problem is that ΔK is generated by a large change in likelihood, but
 131 both increases and decreases in likelihood contribute to this change. Instead, we propose
 132 that only increases should contribute and to this end propose a revised formulation for ΔK
 133 as follows:

$$134 \Delta K_{\text{Revised}} = \text{mean}[\max(L(K) - L(K-1), 0) - \max(L(K+1) - L(K), 0)] / \text{stdev}[L(K)]$$

135 This revised formula is the same as that of the Evanno method when $L(K)$ do not decline with
 136 increasing K , but unlike the Evanno method, only increases and not decreases in likelihood
 137 contribute to the formula. Comparison of the two approaches can be demonstrated clearly
 138 with the following example (Table S2).

139

140 **Table S2**

K	mean*	stdev*	ΔK_{Evanno}	$\Delta K_{\text{Revised}}$
	$L(K)$	$L(K)$		
1	-3000	1	Na	Na
2	-2000	1	1000.0	1000.0

3	-2000	1	3000.0	0.0
4	-5000	1	1000.0	0.0
5	-7000	1	1000.0	0.0
6	-10000	1	Na	Na

* The mean and standard deviation (stdev) values across independent runs of structure for a given K .

141

142

143 Here $K=2$ and $K=3$ both tie for the maximum value of $L(K)$. $K=2$ is thus the best
 144 model because increasing K to 3 does not result in a corresponding increase in $L(K)$.
 145 Nevertheless, ΔK calculated with the Evanno method is higher for $K=3$. Incorrect support
 146 for $K=3$ under the Evanno method arises due to the large drop in $L(K)$ for $K=4$. In contrast,
 147 the revised formula for ΔK correctly chooses $K=2$.

148 Fig. S2 shows both the Evanno and revised ΔK approaches for *Lepidothrix*. Despite
 149 only a modest increase in $L(K)$ from $K=2$ to $K=3$, ΔK_{Evanno} best supports $K=3$, a result
 150 driven largely by the sudden drop in $L(K)$ from $K=3$ to $K=4$. This sudden drop has no effect
 151 in the $\Delta K_{Revised}$ method which best supports $K=2$ for *Lepidothrix*. We conclude that the
 152 slight increase in likelihood from $K=2$ to $K=3$ is not sufficient to support recognition of 3
 153 distinct populations. Nevertheless, we consider results for both $K=2$ and $K=3$ (Fig. 2B).

154

155 **Section 4: Coalescent Modeling**

156 We used composite likelihood modeling implemented in fastSIMCOAL2 2.5 (16) to
 157 compare the fit of three models in which *L. vilasboasi* represents its own unique lineage
 158 without speciation (models T1 to T3: these differ in the topology connecting *L. vilasboasi*,
 159 *L. nattereri*, and *L. iris*) to a hybrid speciation model (model A1) in which *L. vilasboasi*
 160 originates following admixture between *L. iris eucephala* and *L. nattereri* (see Table 1).
 161 Models T1 to T3 each have six parameters: four effective population sizes for the three
 162 species and the common ancestor, and two dates of lineage divergence. Model A1 has the
 163 same parameters, but the second date of lineage divergence is instead the date of genetic
 164 admixture leading to *L. vilasboasi*. In addition, model A1 has a seventh parameter, α , which
 165 measures the proportion of the *L. vilasboasi* genome resulting from *L. nattereri*, while the
 166 contribution from *L. iris* is given by $1-\alpha$. FastSIMCOAL2 takes the observed site frequency
 167 spectrum (SFS; we used the multidimensional SFS for the minor allele at each SNP) for the

168 data and determines the fit of this observed data to each model by simulating a large number
169 of SFS across a range of model parameter values and determining the fit of the observed to
170 the simulated data. We calculated the SFS in Arlequin (17) for Dataset 3 and manually
171 entered the number of non-variable sites in our dataset to the first entry of the SFS. This value
172 was calculated from the proportion of non-variable to variable positions in our dataset
173 multiplied by the number of variable positions included following filtering and thinning of
174 SNPs. We used the neutral rate of 4.6×10^{-9} mutations per generation (18) calculated from
175 whole genomes and pedigree analysis for *Ficedula* flycatchers (belongs to the same order as
176 *Lepidothrix*) to calibrate our model fits. For each model we fitted 144 independent runs, each
177 starting from a different set of random starting parameters drawn from uniform and log-
178 uniform distributions. These distributions ranged from 100 to 1,000,000 (log-normal) for
179 effective population size parameters, 100 to 1,000,000 (uniform) for the time of the basal
180 divergence, 0 to 1 (uniform) for the proportional time of the second event relative to the basal
181 divergence time (uniform), and 0 to 1 for α (uniform). For each set of model parameter values,
182 the fit of the observed data was obtained using 200,000 simulated SFS. Each run used 50
183 EMC loops. We then obtained the maximum likelihood parameter values for each run and
184 re-estimated the likelihood fit to these parameters using 2,000,000 simulated SFS. The larger
185 number of SFS allowed for more precise estimates of the likelihood fit. The best likelihood
186 value and associated set of parameters of the 144 runs was then retained as a close
187 approximation of the true likelihood fit of the data to the model. AIC and Akaike weights
188 calculated from these likelihoods are reported in Table1.







189 The hybrid speciation model gave a much better fit to the data (Table 1) than tree-
190 like models without hybridization. To test whether gene flow occurred after the hybrid
191 speciation event, we next tested a hybrid speciation model in which three additional
192 parameters were added to the model allowing ongoing gene flow among each of the three
193 species (model A3). To reduce the number of migration parameters, we modelled gene flow
194 so that the number of migrants shared between each pair of species per generation was
195 symmetrical. This assumption is justified by the need for model simplicity, though we also
196 note that species pairs share the same parapatric contact zones, and thus the same geographic
197 opportunities for migration assuming equal population density for each species along shared
198 parapatric contact zones. Poor dispersal ability in lowland Neotropical forest birds in general

199 likely means that gene flow only occurs along parapatric contact zones rather than involving
 200 migrants from deep within each species range. We also took the best fit tree topology (model
 201 T3) and added the three migration parameters to this model (model A2). These two additional
 202 models were fit to the data using the same methods as above. All models were then compared
 203 using AIC and Akaike Weights (Table S3). Models with gene flow greatly outperformed
 204 those without, and the hybrid speciation model (model A3) with gene flow outperformed the
 205 gene flow model without hybrid speciation (model A2). These results continue to support the
 206 ancient hybrid speciation event, but suggest that gene flow has occurred following this initial
 207 admixture event. However, unlike our best fit model without ongoing gene flow (model A1),
 208 model parameter estimates of this best fit model had broad confidence intervals (Fig. S4)
 209 suggesting that the signal in the data may not be sufficient to estimate parameters for models
 210 of this complexity

211

212

213 **Table S3.** Support for models in which *Lepidothrix vilasboasi* (V) arises with (A1 to A3) and without
 214 (T1, T2, T3) genetic admixture from *L. nattereri* (N) and *L. iris* (I).

	T1	T2	T3	A1	A2	A3
MODEL						
<i>N</i>	6	6	6	7	9	10
Δ AIC	389.0	480.1	485.7	355.7	7.3	0.0
Akaike weights	0.00	0.00	0.00	0.00	0.03	0.97

215 Models T1, T2, and T3 represent alternative bifurcating tree-like histories without genetic
 216 admixture. Admixture models vary in whether admixture was a point event (A1), involved
 217 admixture over to a protracted period of geneflow (A2), or a combination of the two (A3). Arrows
 218 indicate migration among lineages.

219

220

221 **Section 5: Spectral reflectance**

222 We quantified color differences of crown feathers by measuring spectral reflectance
223 for males of each species of *Lepidothrix*. Wavelengths between 300 and 700 nm were
224 measured using a USB2000 spectrophotometer attached to a PX-2 pulsed xenon light source
225 (Ocean Optics, Dunedin, FL, USA) for crown feathers obtained from 6 museum skins (2
226 for each species). A single feather from each of two individuals per species were stacked
227 beside each other, with feathers slightly overlapping, on black construction paper. Crown
228 feathers were very small and we thus stacked them in order to obtain higher quality
229 measurements (i.e. with less of the black background revealed). We also included two
230 stacked feathers from the crown for the male *L. nattereri* x *L. iris* F1-like hybrid individual
231 (collector number ABG 167). Measurements were taken with a bifurcated micron fiber optic
232 probe (Ocean Optics, Dunedin, FL, USA) held at 45° and 90° angles (two sets of
233 measurements) and 6 mm (45°) or 9 mm (90°) away from the feather surface using probe
234 holders. The spectral reflectance data was generated relative to a RS50 Halon white standard
235 (Stellarnet Inc, Tampa, FL, USA) and a dark standard (measurement taken in a dark box with
236 lamp turned off) to correct for electrical noise. The Ocean View software (Ocean Optics,
237 Dunedin, FL, USA) was used to record the spectrum from each set of stacked feathers with
238 an integration time of 120 ms, repeating this procedure five times for each species at each
239 angle. We used the R package pavo 0.0-1 (19) to average measurements across replicate
240 samples for each species and to smooth spectra.

241 To assess the role of carotenoids in the yellow crown coloration of *L. vilasboasi*, we
242 extracted carotenoids from feathers for two different individuals (separate individuals from
243 the above analyses) using acidified pyridine treatment following the protocol described in
244 (20), and adjusting reagent volumes according to the weight of *Lepidothrix* feathers. After
245 carotenoid extraction these feathers were stacked again and measured with the
246 spectrophotometer following the same procedures described previously.

247

248 **Section 6: Transmission Electron Microscopy**

249 Crown feathers for the three species and the hybrid individual were examined at the
250 nanoscale to test the prediction that the spectral reflectance values for *L. vilasboasi* are
251 produced by a hybrid phenotype of the structural elements of its feathers. Transmission

252 electron microscopy (TEM) was used to measure the morphological characteristics of
253 nanostructural elements known as photonic crystals which can produce structural coloration
254 in visible wavelengths (21, 22). Feather barbs samples were cut from the upper 1cm of the
255 crown feathers (one feather per species) and incubated them in 0.25 M sodium hydroxide and
256 0.1 % Tween-20 for 30 min. The samples were transferred to a solution of 2 parts formic acid
257 to 3 parts ethanol for 3 hours. The samples then were dehydrated by incubating in 100%
258 ethanol twice and 100% propylene oxide once. Then the samples were infiltrated in
259 successive concentrations of 15%, 50%, 70%, and 100% Quetol-Spurr (each step for at least
260 24 hours) and they were cured at 70°C for 48 hours. The samples were cut into cross sections
261 (one section per species) using a diamond knife on a Leica Ultracut UCT ultramicrotome
262 (Leica Microsystems GmbH, Wetzlar, Germany) and each section was stained in osmium
263 and lead citrate. The cross sections were visualized on a Hitachi H7500 (Hitachi, Tokyo,
264 Japan) transmission electron microscope operating at 80 kV at x 10,000, x 20,000 and x
265 25,000. We obtained images for three barbs per section. ImageJ 1.50a software
266 (<http://imagej.nih.gov/ij>) was used to take the following measurements for each image: 1)
267 Number of ordered layers of air and keratin in the spongy matrix measured perpendicular to
268 the barb surface; 2) barb cortex thickness at 10 evenly spaced locations; 3) distance among
269 air pocket centers in the matrix of the spongy layer.

270

271 **References**

- 272 1. Elshire RJ, et al. (2011) A robust, simple genotyping-by-sequencing (GBS) approach
273 for high diversity species. *PLoS One* 6(5):e19379.
- 274 2. Catchen J, Hohenlohe PA, Bassham S, Amores A, Cresko WA (2013) Stacks: an
275 analysis tool set for population genomics. *Mol Ecol* 22(11):3124–3140.
- 276 3. Langmead B, Salzberg SL (2012) Fast gapped-read alignment with Bowtie 2. *Nat*
277 *Methods* 9(4):357–9.
- 278 4. Danecek P, et al. (2011) The variant call format and VCFtools. *Bioinformatics*
279 27(15):2156–2158.
- 280 5. Hammer O, Harper DTA, D RP (2001) Past: Paleontological statistics software
281 package for education and data analysis. *Palaeontol Electron* 4(1):9.
- 282 6. Pritchard JK, Stephens M, Donnelly P (2000) Inference of population structure using
283 multilocus genotype data. *Genetics* 155(2):945–59.

- 284 7. Evanno G, Regnaut S, Goudet J (2005) Detecting the number of clusters of
285 individuals using the software STRUCTURE: A simulation study. *Mol Ecol*
286 14(8):2611–2620.
- 287 8. Earl D a., vonHoldt BM (2012) STRUCTURE HARVESTER: a website and
288 program for visualizing STRUCTURE output and implementing the Evanno method.
289 *Conserv Genet Resour* 4(2):359–361.
- 290 9. Huson DH, Bryant D (2006) Application of phylogenetic networks in evolutionary
291 studies. *Mol Biol Evol* 23(2):254–267.
- 292 10. Hudson RR, Slatkin M, Maddison WP (1992) Estimation of levels of gene flow from
293 DNA sequence data. *Genetics* 132:583–589.
- 294 11. Malinsky M, Trucchi E, Lawson D, Falush D (2016) RADpainter and
295 fineRADstructure: population inference from RADseq data. *bioRxiv* (Mm):57711.
- 296 12. Haffer J (1997) Contact zones between birds of southern Amazonia. *Ornithol*
297 *Monogr* 48:281–305.
- 298 13. Gompert Z, Alex Buerkle C (2010) Introgress: A software package for mapping
299 components of isolation in hybrids. *Mol Ecol Resour* 10(2):378–384.
- 300 14. Templeton AR, Crandall KA, Sing CF (1992) Cladistic Analysis of Phenotypic
301 Associations With Haplotypes Inferred From Restriction Endonuclease Mapping and
302 DNA Sequence Data. III. Cladogram Estimation. *Genetics* 132:619–633.
- 303 15. Paradis E (2010) Pegas: An R package for population genetics with an integrated-
304 modular approach. *Bioinformatics* 26(3):419–420.
- 305 16. Excoffier L, Dupanloup I, Huerta-Sánchez E, Sousa VC, Foll M (2013) Robust
306 demographic inference from genomic and SNP data. *PLoS Genet* 9(10):e1003905.
- 307 17. Excoffier L, Laval G, Schneider S (2005) Arlequin (version 3.0): An integrated
308 software package for population genetics data analysis. *Evol Bioinform Online* 1:47–
309 50.
- 310 18. Smeds L, Qvarnström A, Ellegren H (2016) Direct estimate of the rate of germline
311 mutation in a bird. *Genome Res* 26(9):1211–1218.
- 312 19. Maia R, Eliason CM, Bitton P-P, Doucet SM, Shawkey MD (2013) pavo : an R
313 package for the analysis, visualization and organization of spectral data. *Methods*
314 *Ecol Evol* 4:906–913.
- 315 20. McGraw KJ, Hudon J, Hill GE, Parker RS (2005) A simple and inexpensive
316 chemical test for behavioral ecologists to determine the presence of carotenoid
317 pigments in animal tissues. *Behav Ecol Sociobiol* 57(4):391–397.
- 318 21. Eliason C, Shawkey M (2012) A photonic heterostructure produces diverse
319 iridescent colours in duck wing patches. *J R Soc Interface* 9:2279–2289.
- 320 22. Eliason CM, Maia R, Shawkey MD (2015) Modular color evolution facilitated by a
321 complex nanostructure in birds. *Evolution* 69(2):357–367.

322

323

324

325

326

327

328

329

330

331

332

333 **Figure S1**

334 The decay of linkage disequilibrium (r^2) as a function of physical distance for three species of
335 *Lepidothrix* manakin. Only shown are loci with data for 12 to 15 individuals for each species. The
336 two red lines indicate the expected r^2 value (i.e. $1/n$) for $n=12$ and 15 individuals when linkage
337 disequilibrium is absent. Decay curves for all three species reach the expectation in less than 5,000
338 bp. *L. nattereri* has more SNPs present because it has a much larger pool of individuals sequenced.

339

340 **Figure S2**

341 Results of the Bayesian analysis of population structure under different numbers of populations
342 (K). A) change of $L(K)$ with increasing K . B) the ΔK_{Evanno} (blue line) and $\Delta K_{Revised}$ (orange line)
343 statistic for $K=2$ to $K=5$. See Section 3 for details.

344

345 **Figure S3**

346 Analysis of hybrid index and observed heterozygosity. A) heterozygosity and hybrid index for
347 populations color coded as in Fig. 2B. Heterozygosity is calculated for SNPs from Dataset 1 for
348 which parental populations (*Lepidothrix iris eucephala*: blue; *L. nattereri* east of the
349 Tapajós/Juruena Rivers: Green) have less than 50% missing data and allele frequency differences
350 greater than 0.25. Box plots (with whiskers representing the range between the 0.025 and 0.975
351 quantiles that encompass 95% of the data) are shown for 1000 simulated individuals for each of
352 four early generation hybrids. The hybrid indexes for these individuals are shown at their
353 expectation of 0.5 for F_1 and F_2 , 0.25 for $F_1 \times L. nattereri$, and 0.75 for $F_1 \times L. iris$. B) histogram of
354 hybrid indices for individuals from contact zone birds (all individuals from localities where at least
355 1 individual had a hybrid index between 0.05 and 0.95. C) histogram of hybrid indices for *L.*
356 *vilasboasi* individuals. Hybrid indices obtained from our analysis of structure with two populations
357 inferred.

358

359

360

361 **Figure S4**

362 Maximum likelihood parameter estimates of the best fit models without (A) and with (B) migration
363 among species. The proportion of individuals of *L. nattereri* and *L. iris* origin in the founding
364 population of *L. vilasboasi* are shown by α and $1-\alpha$ respectively. The number of migrants (N_m) per
365 generation among species are shown. Thickness of the vertical lines correspond to effective
366 population size estimates which are stated in units of thousands.

367

368 **Figure S5**

369 Electron scanning micrographs of whole barb sections ($\times 10,000$) for *L. irisi* (A), *L. nattereri* (B), *L.*
370 *vilasboasi* (C) and *L. iris* \times *L. nattereri* hybrid. Irregular translucent black lines and spots are
371 sectioning artifacts and don't represent actual structures.

372

373 **Figure S6**

374 Detail of the geographic range of *Lepidothrix vilasboasi* and surrounding congeners. Numbered
375 arrows as follows. 1) Location of syntopy of *L. vilasboasi* and *L. iris* on the east bank of the
376 Jamanxim River indicating that this river – which is 70 to 100 m wide at this latitude – is not an
377 absolute barrier, and that these species at least occasionally come into geographic contact in the
378 vicinity of the river. 2) Location of hybrid sample BR163-064 with admixture proportions from the
379 program Structure ($K = 3$) of 85% *L. iris* and 14% *L. nattereri*. This individual occurs north of the
380 Cachimbo Range and west of the Jamanxim River (which at this latitude is as narrow as 10m) with
381 *L. vilasboasi* sampled on the same side of this river just 130km to the north. No major river
382 barriers (i.e. with widths > 25 m) occur between *L. vilasboasi* and this location. A parapatric contact
383 zone between *L. iris* and *L. vilasboasi* is almost certain to occur somewhere in the region
384 encompassed by the dotted red contour. 3) This arrow indicates a lowland forested corridor that
385 goes around the northern edge of the Cachimbo Range. The lack of river barriers and the presence
386 of uninterrupted forest through this corridor strongly suggest that *L. vilasboasi* and *L. nattereri*
387 come into geographic contact in this poorly explored region. In addition, the Cachimbo Range itself
388 typically rises only 100 to 250 meters above the surrounding lowlands and is unlikely to present an
389 absolute barrier to geneflow. We suspect that parapatric contact between *L. vilasboasi* and *L.*

390 *nattereri* occurs along its northern half (dashed green contour) as it does between *L. nattereri* and
391 *L. iris* along its southern half (dashed purple contour). Black circles show collecting localities for
392 genomic samples in this study. Black arrows indicate sample sites of *L. nattereri* along both banks
393 of the Teles Pires. The Cachimbo range is shown by inverted V's.

394

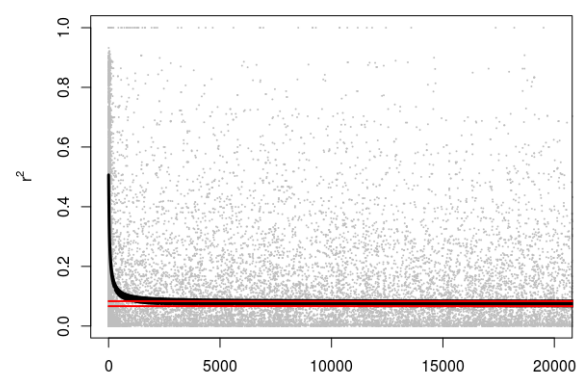
395

396 **Figure S7**

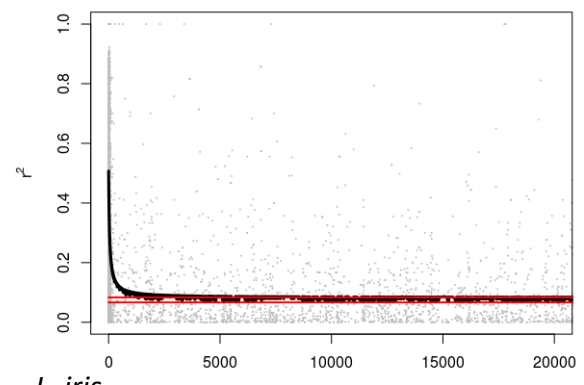
397 Possible scenario leading to the yellow crown of *L. vilasboasi*. *L. iris* and *L. nattereri* produce a
398 hybrid swarm in which the intermediate nature of the nanostructural elements of the crown barb
399 result in a loss of reflectance. The duller appearance of the crown renders males less showy at
400 their dark forest interior lekks. Sexual selection then resulted in the thickening of the crown barb
401 cortex and deposition of carotenoids to the cortex resulting in the yellow crown coloration of *L.*
402 *vilasboasi*. Feather shown are from their respective species. The dull whitish/gray feather
403 representing the hybrid population is a *L. vilasboasi* crown feather for which carotenoids were
404 extracted and which we assume closely matches the ancestral hybrid swarm prior to deposition of
405 carotenoids.

Figure S1

L. nattereri



L. villasboasi



L. iris

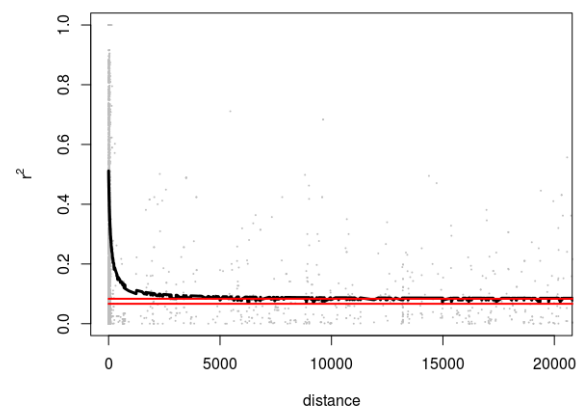
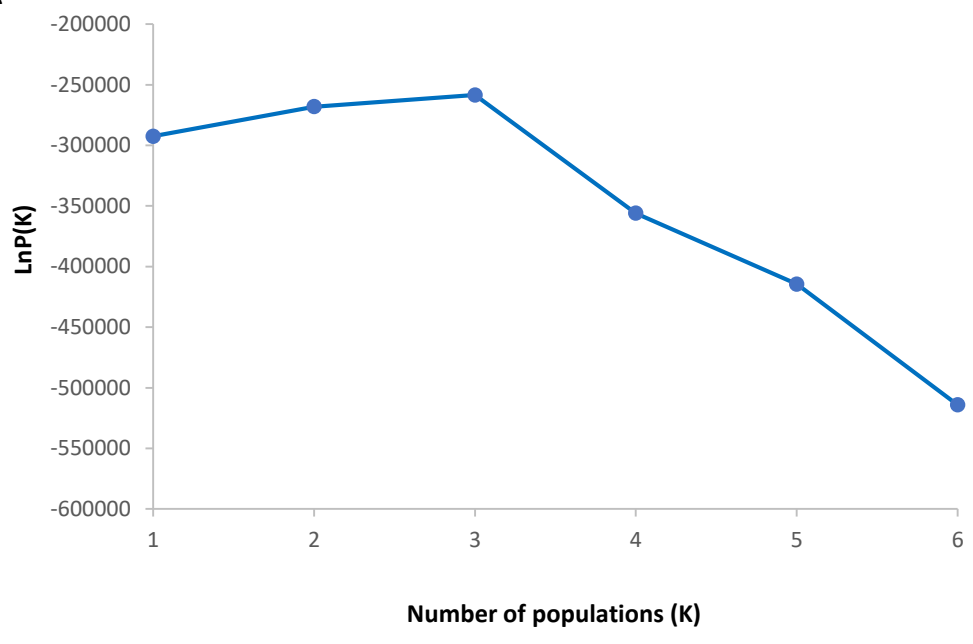


Figure S2

A



B

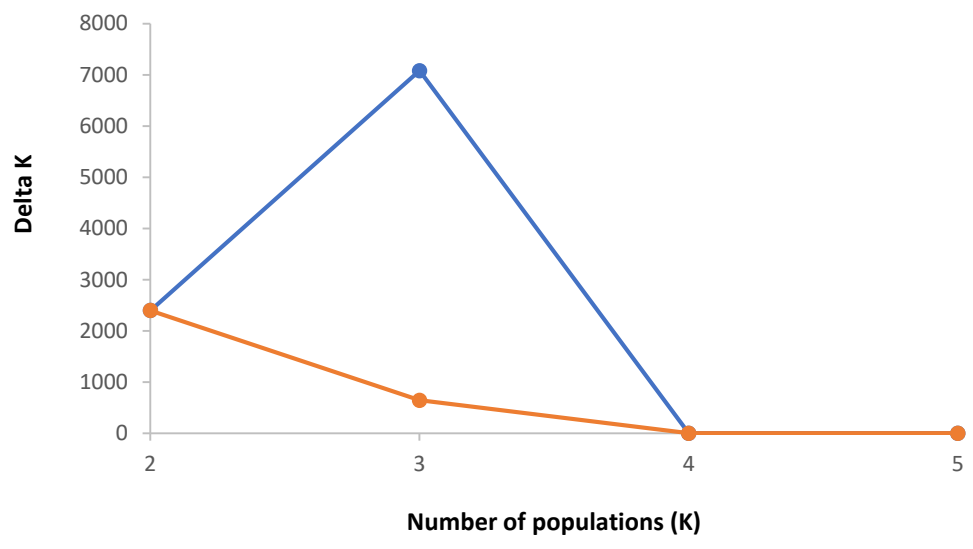


Figure S3

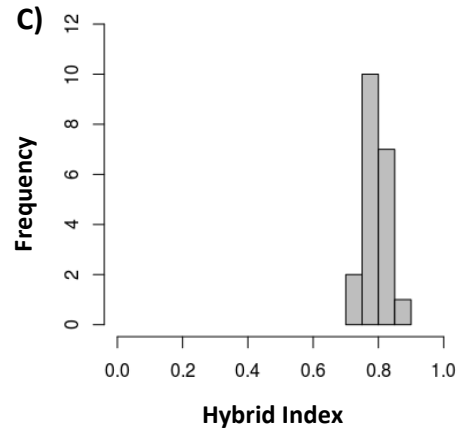
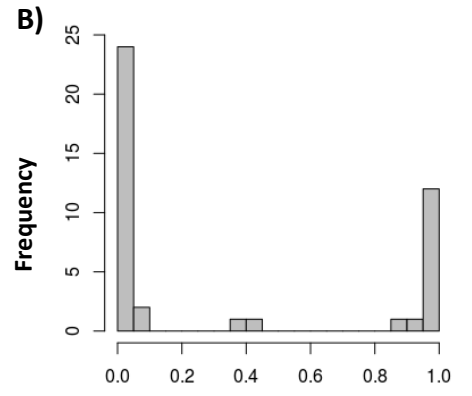
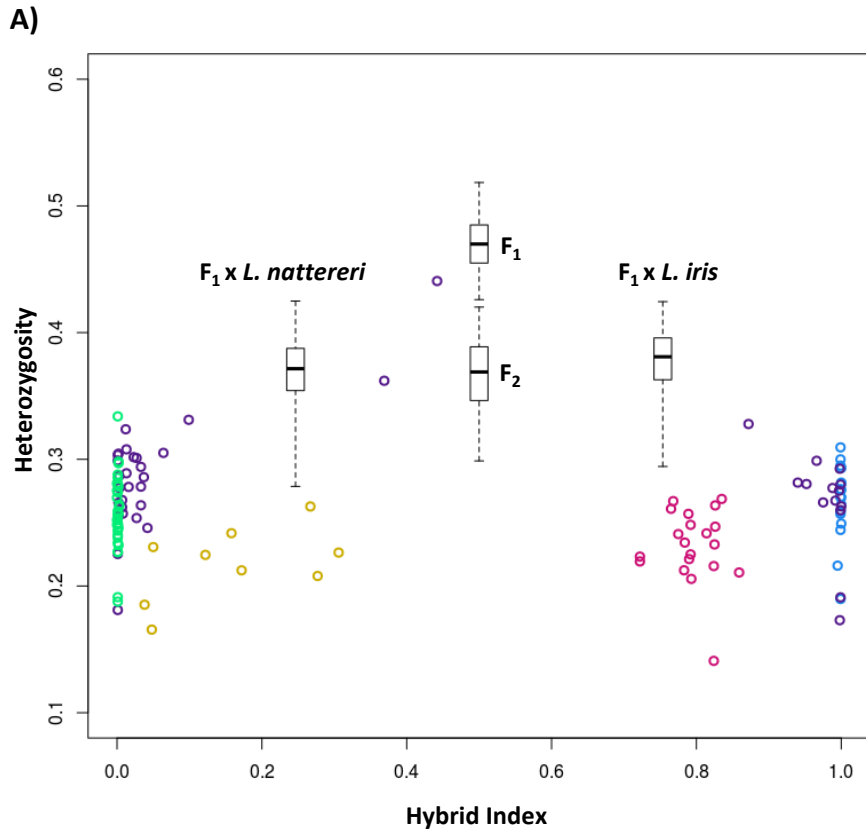


Figure S4

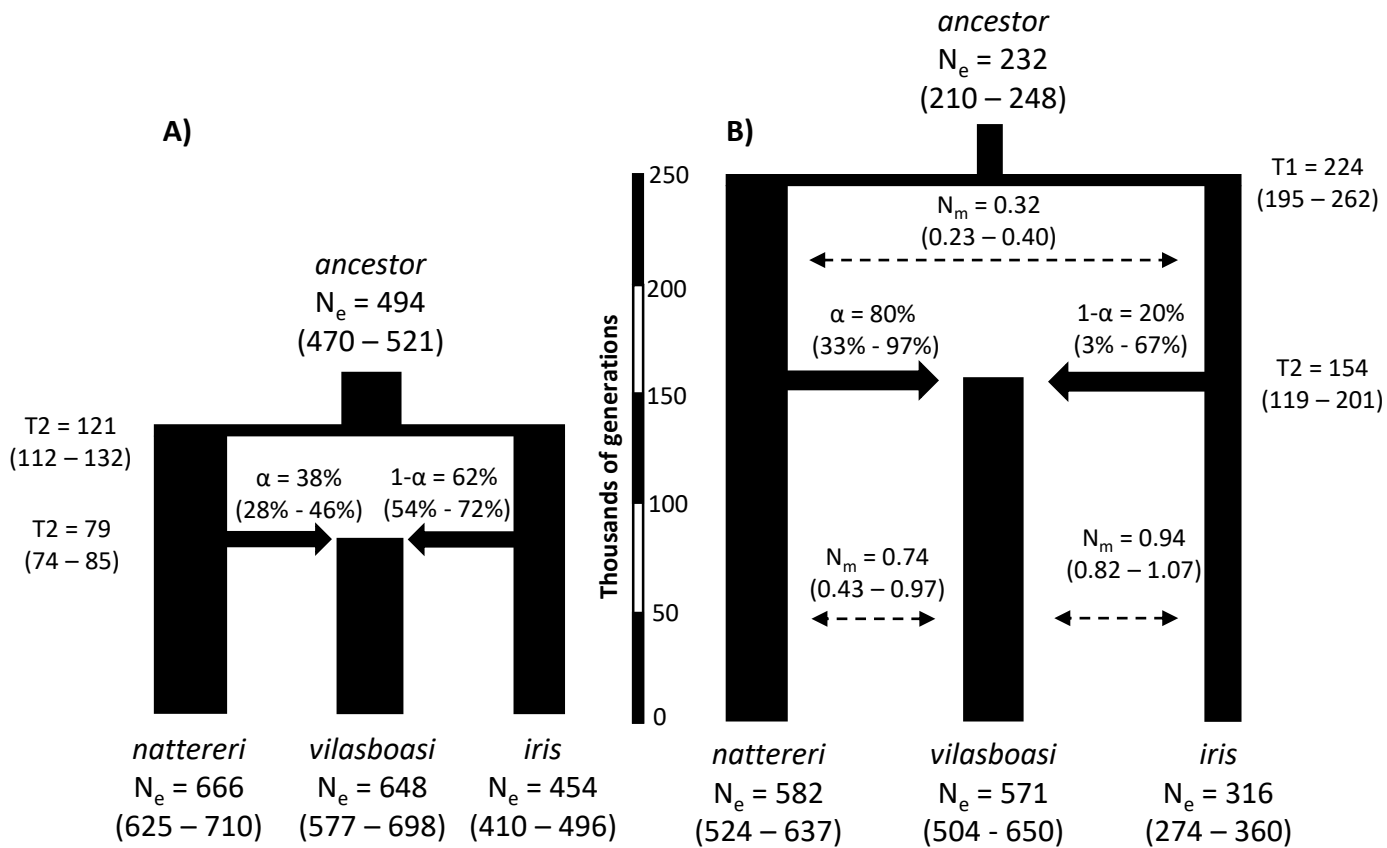


Figure S5

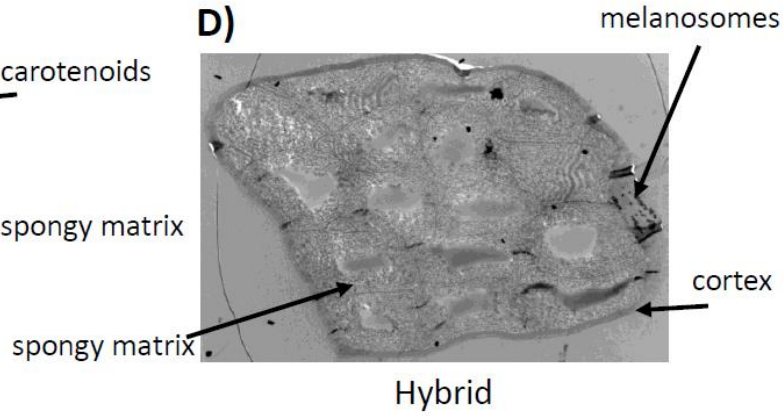
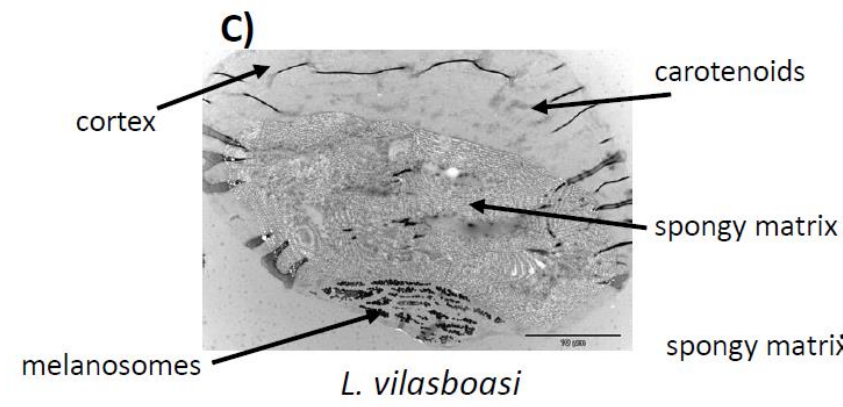
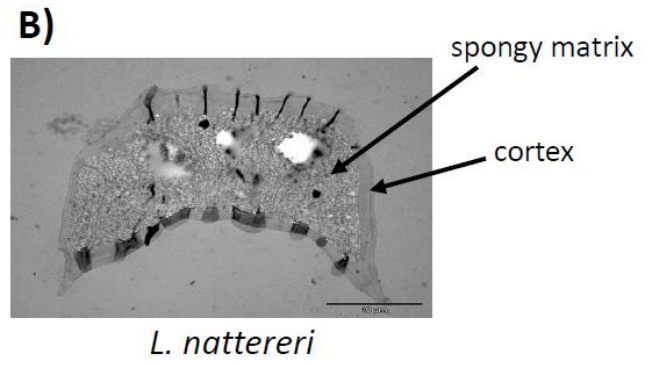
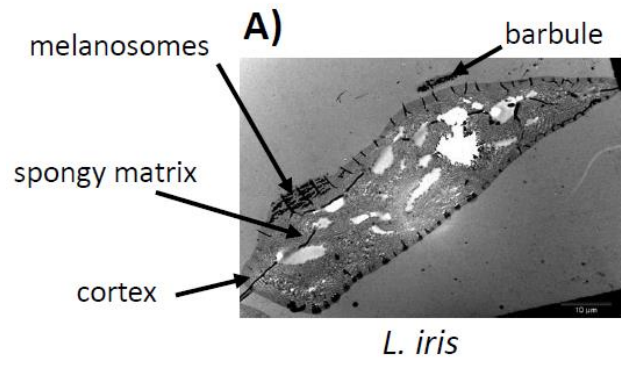


Figure S6

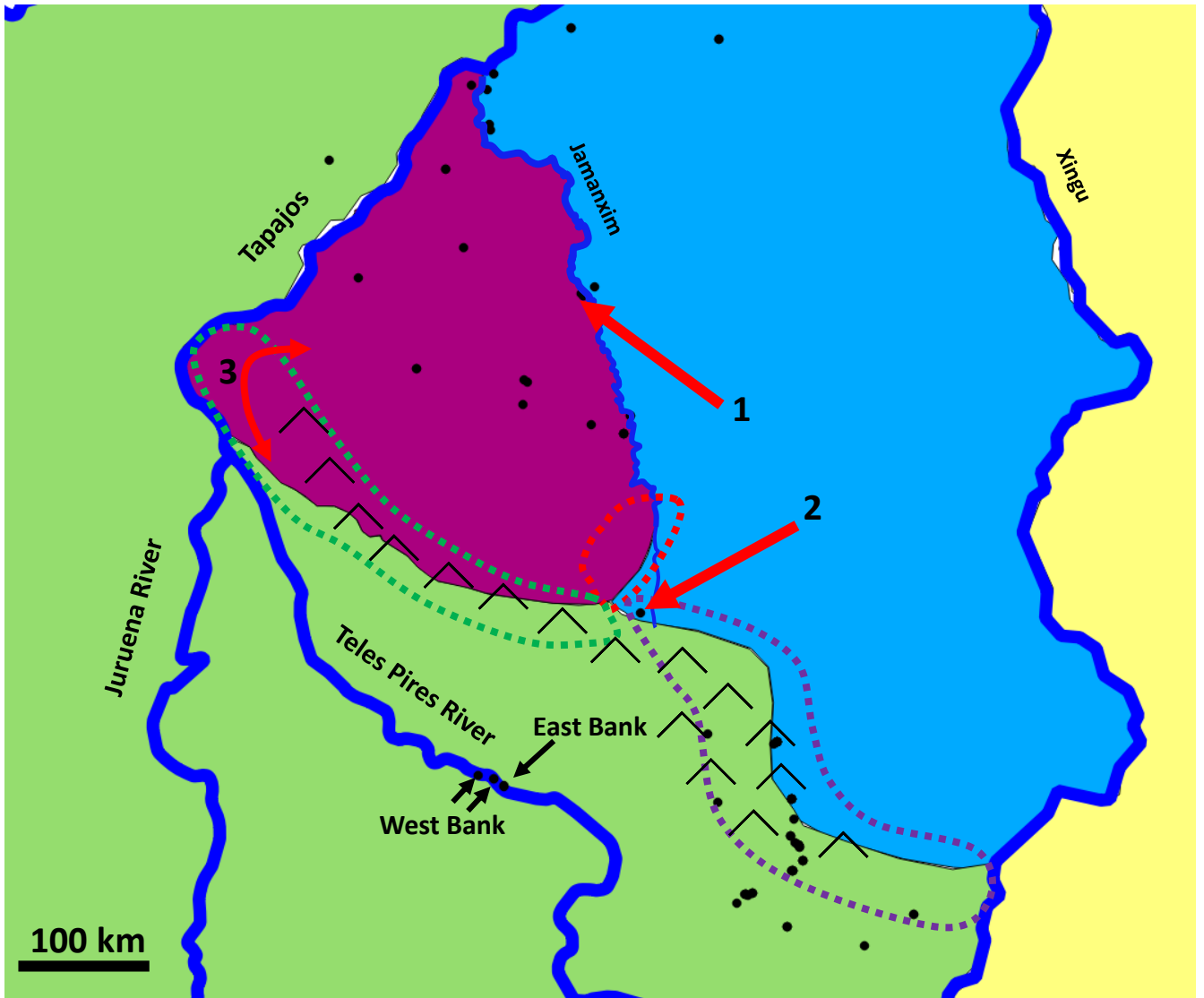


Figure S7

